Geophysical Research Letters

RESEARCH LETTER
10.1029/2025GL118605

Strengthening of Labrador Sea Overturning Linked to Subsurface Freshening Over Recent Decades

Feili Li[1], **Yao Fu**[2], **Tillys Petit**[3], **and Sijia Zou**[1]

[1]State Key Lab of Marine Environmental Science & College of Ocean and Earth Sciences, Xiamen University, Xiamen, China, [2]University of South Florida, Tampa, FL, USA, [3]National Oceanography Centre, Southampton, UK

Key Points:

- Labrador Sea overturning changes are associated with time-dependent density compensation imposed by large thermal and haline anomalies
- The strengthening of Labrador Sea overturning during the most recent decade is linked to subsurface fresh anomalies at boundary currents

Supporting Information:

Supporting Information may be found in the online version of this article.

Correspondence to:

S. Zou,
szou@xmu.edu.cn

Citation:

Li, F., Fu, Y., Petit, T., & Zou, S. (2026). Strengthening of Labrador Sea overturning linked to subsurface freshening over recent decades. *Geophysical Research Letters*, *53*, e2025GL118605. https://doi.org/10.1029/2025GL118605

Received 4 AUG 2025
Accepted 18 DEC 2025

Abstract The Labrador Sea is a key formation site for dense waters that contribute to the lower limb of the Atlantic meridional overturning circulation (AMOC). Recent observations have revealed a distinctly weak overturning in this basin, attributed to compensating effects of temperature and salinity anomalies on density. However, it remains unclear whether these effects are consistent under varying hydrographic conditions and whether they subsequently impact overturning variability. By combining moored observations and historical hydrographic data, we demonstrate a coherent response of the Labrador Sea overturning to salinity anomalies over recent decades. Notably, a strengthened overturning in the late 2010s can be attributed to subsurface fresh anomalies advected into the basin by the boundary currents, which are linked to large-scale freshening that began in the late 2000s. Our findings underscore the necessity of continuously monitoring boundary salinity and temperature anomalies to capture ongoing changes in the Labrador Sea.

Plain Language Summary The Atlantic Meridional Overturning Circulation, a key constituent of the climate system, exhibits substantial interannual-decadal variability that is often linked in models to density fluctuations in the Labrador Sea. However, observations reveal weak overturning variability in the Labrador Sea, as temperature and salinity anomalies largely compensate to dampen density changes. Yet how this compensation evolves under changing hydrographic conditions—particularly with enhanced freshwater input from high latitudes—and its impact on overturning strength remain unclear. By combining moored observations and historical hydrographic data, we show that temperature and salinity variations critically regulate Labrador Sea density anomalies and overturning variability over the past two decades. Particularly, we find a strengthened overturning in the late 2010s that is linked to the advection of fresh subsurface waters into the basin, likely originating from an extreme freshening event developed since around the late 2000s. Our findings underscore the subtle yet significant role of boundary-driven salinity changes in modulating Labrador Sea density and thus overturning.

1. Introduction

Variability in the Atlantic Meridional Overturning Circulation (MOC) has been linked to varying strength of deep convection and/or water mass transformation in the Labrador Sea (e.g., Jackson et al., 2016; Yeager & Danabasoglu, 2014; Yeager et al., 2021). However, recent observations of the subpolar overturning strength from the transatlantic OSNAP (the Overturning in the Subpolar North Atlantic Program) array found a minimal Labrador Sea contribution during the mid 2010s (Lozier et al., 2019). The weak overturning in the Labrador Sea is consistent with previous observational estimates of the overturning strength based on hydrographic transects from the early 1990s (Fu et al., 2020; Pickart and Spall, 2007), a period of much stronger deep convection (e.g., Yashayaev & Loder, 2016). Such consistency follows a constrained overturning in the Labrador Sea that results from the compensating effects of temperature and salinity anomalies within the basin (Mackay et al., 2020; Pickart & Spall, 2007; Zou et al., 2020, 2024). Specifically, wintertime convection generates large temperature and salinity anomalies, leading to the transformation of the warm and salty inflowing waters at the West Greenland Current (WGC) to the relatively colder and fresher outflowing waters at the Labrador Current (LC). The concurrent freshening (salty-to-fresh transformation) and cooling (warm-to-cold transformation) have opposing effects on density that lead to a minimal density anomaly (i.e., a weak light-to-dense water mass transformation) and thus a weak overturning in the Labrador Sea (~3 Sv; Figure 1). What remains unclear is whether the strength of density compensation varies with time and subsequently impacts the overturning strength.

10.1029/2025GL118605

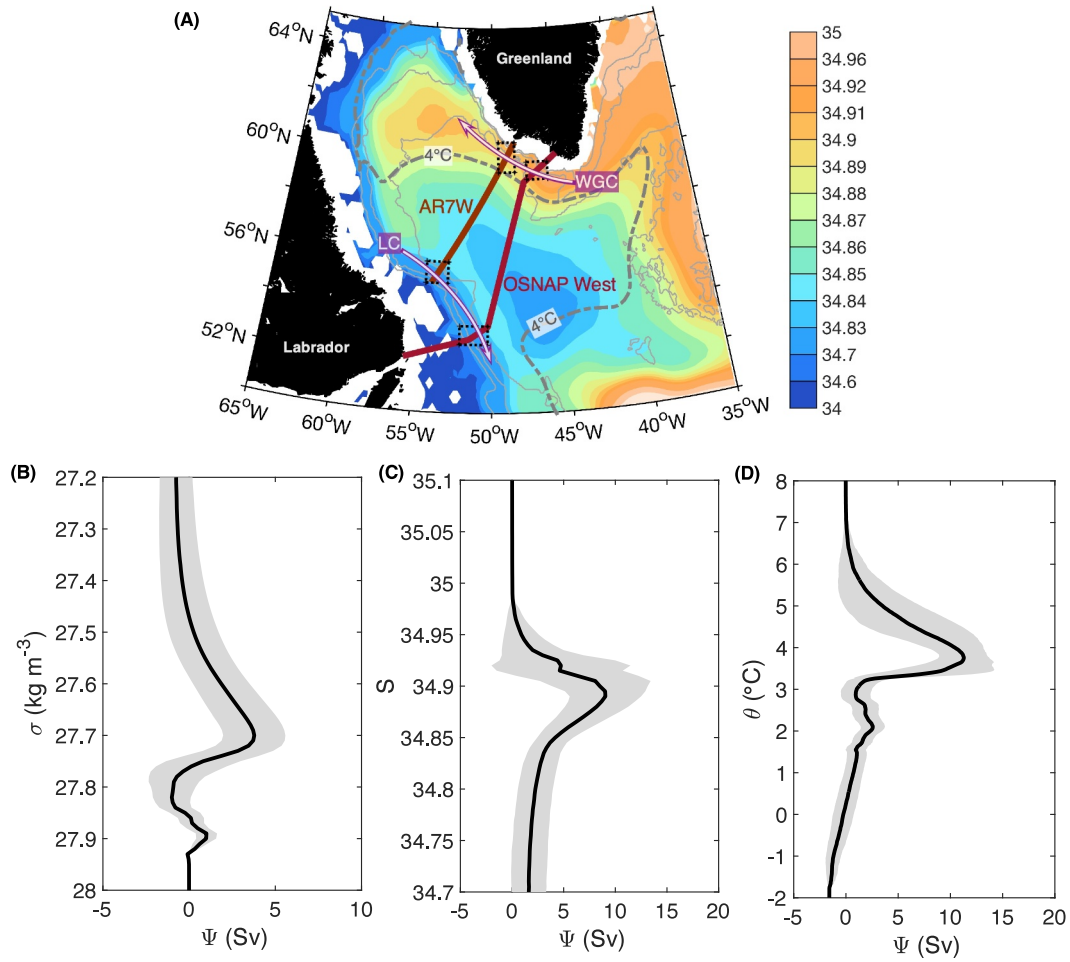

Figure 1. (a) Mean salinity (color shading) and temperature (gray dashed contour) fields at the subsurface Labrador Sea (200–500 m) from World Ocean Atlas 2018, superimposed by the location of the AR7W and OSNAP West sections. Gray thin lines are the 1,000 m-, 2,000 m-, and 3,000 m-isobaths. The inflowing and outflowing boundary currents are labeled with white arrows. WGC, West Greenland Current; LC, Labrador Current. Black dotted boxes on the sections indicate where EN4 profile data are collected for the analysis. (b–d) Time-mean overturning streamfunction across the Labrador Basin (solid black lines with the envelope being the monthly standard deviation) in potential density (integrated from the bottom upward), salinity, and potential temperature spaces, respectively. Data are from the OSNAP West array during 2014–2020.

Recent observations show a notable strengthening of the Labrador Sea overturning lately, with an increase by ∼50% from 2014–2016 to 2018–2020 (Fu et al., 2023a). The change happens in conjunction with an extreme freshening throughout the subpolar North Atlantic since early 2010s, likely originated from the Labrador Sea (Haine et al., 2023; Holliday et al., 2020). Alongside this salinity change, there are also large changes in temperature in the region (Chafik et al., 2023; Yashayaeve, 2024), both of which can exert a strong influence on Labrador Sea density across the interannual to decadal time scales (e.g., Desbruyères et al., 2019; Jackson et al., 2016; Menary et al., 2016; Robson et al., 2016; Yashayaev, 2024). Yet it is not clear whether the observed strengthening of the Labrador Sea overturning is a response to recent large-scale changes in salinity and/or temperature in the subpolar region, and if so, how this response is established.

In this study, we use observational records to (a) assess how hydrographic changes in the Labrador Sea impact its overturning variability, and (b) investigate how such impact is established by isolating temperature versus salinity effects. We begin with the OSNAP record to focus on observed interannual changes and then incorporate historical hydrographic data to investigate decadal-scale changes.

2. Data and Methods

2.1. OSNAP Data

Observational record used in this study includes the monthly gridded velocity, temperature, and salinity products from the OSNAP West array between July 2014 and June 2020 (Fu et al., 2023b). The gridded data have a horizontal resolution of ∼1/4° and a vertical resolution of 20 m. Gridded velocity and property fields at the boundaries are obtained directly by interpolating the moored observations from the boundary arrays. In the interior basin, the geostrophic velocities are obtained from dynamic height moorings at each side of the basin by referencing to the time-mean surface altimetry velocity. Then, a spatially uniform velocity is applied at each month to match the net throughflow from the Davis Strait into the Labrador Sea (1.6 Sv; Curry et al., 2011). Property fields for the interior basin for the upper 2,000 m are obtained through an objective analysis method (e.g., Bretherton et al., 1976), which incorporate data from the moorings and Argo profiles, along with the World Ocean Atlas 2018 climatology (Locarnini et al., 2019; Zweng et al., 2019). Below 2,000 m, data from the full-depth CTD occupations during the summers of 2014 and 2016 are used. More details on the calculation methods can be found in Li et al. (2017), Lozier et al. (2019) and Fu et al. (2023a).

2.2. EN4 Data

Hydrographic data are from UK Met Office Hadley Center Enhanced Ocean Data Assimilation and Climate Prediction (ENACT) archive version 4.2.2 data set (EN.4.2.2, Good et al., 2013). The salinity and temperature profiles in the vicinity of the AR7W or OSNAP West sections and within the boundary currents are selected, with temporal resolutions ranging from days to weeks (dashed boxes in Figure 1a). Depth-weighted mean value is calculated for those profiles, which are then used to yield the domain averages. In addition, the monthly gridded salinity data from EN4 are used to show the salinity distribution change during the most recent decade.

2.3. Repeat Hydrographic Sections

The hydrographic sections across the Labrador Sea are composed of the WOCE line AR7W and the OSNAP West line (Figure 1a). The AR7W line, running from the Labrador shelf to the western shelf of Greenland, is occupied almost annually in the late spring and early summer. The occupation along this line is part of the WOCE program and is still ongoing. The OSNAP West line follows the OSNAP array position in the basin from the Labrador coast to the Greenland coast and deviates slightly from the AR7W line in position. Salinity and temperature measurements from the full-depth CTD occupations between 1990 and 2016 are used in this study.

2.4. Inverse Method

The absolute geostrophic velocity field across the hydrography section is obtained via an inverse method (Wunsch, 1996), applied to an enclosed oceanic volume bounded by the subpolar sections nominally at ∼60°N and the subtropical sections at ∼25°N (Fu et al., 2020). All sections have been occupied in the same or adjacent years for multiple times since 1990. By considering transports across the hydrographic sections, a box inverse model is formulated as a set of conservation equations for different properties (including volume, heat, and salt) in different vertical layers bounded by neutral density surfaces as well as in the whole box. In matrix form, the equations can be expressed as

$$Ax = b, \tag{1}$$

where A consists of grid cell areas of cross-sectional velocity bins multiplied with property concentration within each velocity bin and horizontal areas of neutral density surfaces multiplied with the area-weighted mean property concentration at density surfaces, x consists of the unknowns including reference geostrophic velocity and vertical velocity across density surfaces, and b consists of transports of properties by relative geostrophic velocity and Ekman transport. Additional constraints include satellite altimetry as the initial guess for the reference velocity.

The solution to the box inverse model provides a best estimate of the reference velocity to the relative geostrophic velocities derived from temperature and salinity profiles measured across the sections. Together, the absolute velocities and thus transports across the Labrador Sea sections are obtained (Figures S1 and S2 in Supporting

Information S1). The readers are referred to Fu et al. (2020) for details on the calculations and validations of the inverse model results.

2.5. Overturning Strength

We define the overturning strength as the maximum of the overturning streamfunction in density space (denoted as MOC_σ) along a cross-basin section (AR7W or OSNAP West), following Lozier et al. (2019).

$$MOC_\sigma = \max[\Psi(\sigma)] = \max\left[-\int_{\sigma_{max}}^{\sigma}\int_{x_e}^{x_w} v(x,\sigma)\,dx\,d\sigma\right], \quad (2)$$

where $v(x,\sigma)$ is the volume transport per unit length per density layer in the direction normal to the section (positive is into the Labrador Basin), σ is potential density referenced to the sea surface, and the double intergral is taken over all σ surfaces at intervals of 0.01 kg m^{-3} (from high to low densities) and between the western and eastern boundaries. In steady state, $\Psi(\sigma)$ equals to the strength of light-to-dense water mass transformation rate (i.e., volume transport across isopycnals) occurring northwest of the section (Speer & Tziperman, 1992; Walin et al., 1982).

Following previous studies (Xu et al., 2016; Zou et al., 2020), we calculate the transport streamfunction in salinity S (potential temperature θ) space by accumulating volume transport across isohalines (isotherms), with a uniform bin size of $\Delta S = 0.005$ ($\Delta\theta = 0.02$°C). The maximum streamfunction is denoted as MOC_S (MOC_θ), that is

$$MOC_S = \max[\Psi(S)] = \max\left[\int_{S_{max}}^{S}\int_{\theta_{min}}^{\theta_{max}} v^*(\theta^*,S^*)\,d\theta^*dS^*\right], \quad (3)$$

$$MOC_\theta = \max[\Psi(\theta)] = \max\left[\int_{\theta_{max}}^{\theta}\int_{S_{min}}^{S_{max}} v^*(\theta^*,S^*)\,dS^*d\theta^*\right]. \quad (4)$$

here, $\Psi(S)$ and $\Psi(\theta)$ represent the transport streamfunctions in salinity and potential temperature coordinates, respectively. The double integral is taken from high to low S (θ) and across all θ (S) surfaces. In steady state, $\Psi(S)$ equals to the diahaline transformation rate (i.e., net volume transport across salinity surface) occurring northwest of the section, while $\Psi(\theta)$ denotes the diathermal transformation rate (i.e., net volume transport across temperature surface).

3. Results

3.1. Strengthening of Labrador Sea Overturning in 2014–2020

The time-mean overturning in the Labrador Sea, that is MOC_σ mostly reflects the diapycnal water mass transformation within the basin at time scales longer than a few years (Zou et al., 2024), which is associated with concurrent changes in the strength of warm-to-cold and salty-to-fresh transformations (i.e., MOC_θ and MOC_S respectively). The mean MOC_σ during 2014–2020 is 3.8 ± 0.2 Sv (plus/minus one standard error), occurring at $\sigma = 27.7$ kg m^{-3}. As shown in Figure 1, despite a relatively modest diapycnal transformation, substantially stronger transformation occurs across temperature and salinity surfaces in the basin: the 2014–2020 mean MOC_θ is 11.3 ± 0.3 Sv (at $\theta = 3.76$°C), while the 2014–2020 mean MOC_S is 9.0 ± 0.4 Sv (at $S = 34.89$). These results underscore the significant constraint by density-compensating thermal and haline anomalies on the mean MOC_σ in the Labrador Sea (Pickart & Spall, 2007; Zou et al., 2020).

The MOC_σ, MOC_θ and MOC_S time series exhibit considerable yet distinct variability from 2014 to 2020 (Figure 2). There is similar variability in MOC_θ and MOC_σ on monthly time scales, which explains 84% and 70% of the respective total variability across all the observable time scales. By comparison, MOC_S is marked by a significant decline during that period, with its monthly variability explaining only 40% of the total variability. Accordingly, the monthly MOC_σ is significantly related to the MOC_θ ($r = 0.6$, $p < 0.001$; detrended data), with a weaker correlation for MOC_S ($r = -0.3$, $p = 0.028$; detrended data), suggesting a more important role of temperature on monthly time scales. By comparison, a stronger linkage between MOC_S and MOC_σ seems to exist concerning the year-to-year changes ($r = -0.8$, $p = 0.09$). The decline in the MOC_S is characterized by a large

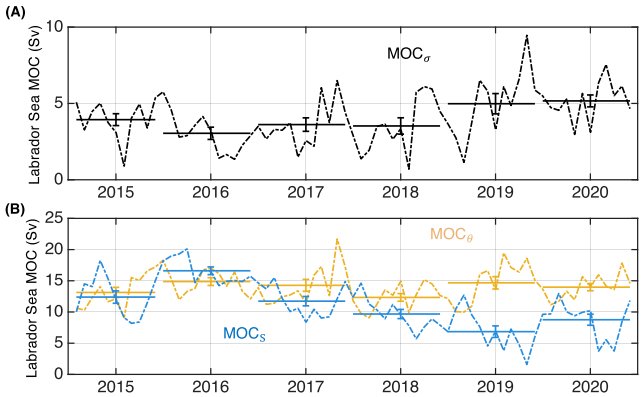

Figure 2. Labrador Sea MOC estimates across the OSNAP West section in panel (a) potential density coordinates, and (b) potential temperature and salinity coordinates, respectively. The *y*-axis ranges differ between (a, b). Horizontal lines indicate the annual averages (July to June), with the vertical bars representing the uncertainty of each annual estimate (plus/minus one standard error obtained from the monthly values).

reduction from 2016 to 2019 (by 9.7 Sv in the annual averages) and that is accompanied by a clear increase in the MOC_σ between the years (by 2.0 Sv), both of which are statistically significant according to the error bars (Figure 2). By contrast, the year-to-year changes in the MOC_θ are overall negligible during 2014–2020 (being ∼1–2 Sv or < 20% of its overall mean strength).

Collectively, the above results point to salinity anomalies as the key driver of interannual MOC_σ variability over the observed period. Previous work shows MOC_σ in the Labrador Sea is critically influenced by density changes in the boundary currents (e.g., Li et al., 2021; Roussenov et al., 2022). We therefore explore the hypothesis that a major change occurred in the salinity anomalies along the boundary current that have led to the 2014–2020 strengthening of the Labrador Sea overturning.

3.2. Distinct Effect of Boundary Fresh Anomalies

In the mean state, most of the inflowing waters in the WGC are saltier than the outflowing waters in the LC at the same depths (e.g., Figure S3 in Supporting Information S1). The spatial pattern results in a salinity gradient between the boundary currents (i.e., salinities at WGC vs. LC) that corresponds to a salty-to-fresh transformation within the basin and thus a positive MOC_S. Clear salinity changes of the inflowing waters at the WGC between 2016 and 2019 can be seen in Figures 3a and 3b. Those waters are relatively salty during 2016 especially in the upper layers (with maximum S ∼ 34.96 at σ ∼ 27.7 kg m^{-3}), leading to a large salinity gradient with the outflowing waters (primarily with S ∼ 34.84–34.9 at σ ∼ 27.7 – 27.8 kg m^{-3}). By 2019, the inflowing waters had freshened considerably (with a local maximum S ∼ 34.91 at σ ∼ 27.7 kg m^{-3}), with salinities that are now comparable to some of the outflowing waters. Salinities of the outflowing waters are similar between the 2 years. Therefore, the decreased WGC salinity from 2016 to 2019 led to a reduced salinity gradient between the inflowing and outflowing boundary currents.

The reduced salinity gradient has an impact on the transport structure in salinity coordinate, which correspond to a weakened MOC_S (Figure 3c). In 2016, the transport of inflowing waters concentrates at the isohalines of 34.9–34.94, whereas the transport of outflowing waters occurs primarily at fresher surfaces (S < 34.9). The difference results in a net inflow (outflow) at S > 34.9 (<34.9) in 2016, corresponding to MOC_S of ∼15 Sv reached at S = 34.9. By contrast, the transports of inflowing and outflowing waters in 2019 occur at more comparable salinities (S < 34.9), leading to strong cancellation of transport along isohalines and thus a weaker MOC_S (∼5 Sv at S = 34.9). Therefore, it indicates a dominant role of inflow salinity anomaly in modulating MOC_S, with positive (negative) anomalies producing an increase (reduction) in the net transport in salinity space and hence a strengthened (weakened) MOC_S.

The relationship between boundary salinities and MOC_S is robustly strong over interannual time scales during 2014–2020 (Figure S4 in Supporting Information S1). In particular, the subsurface WGC salinity at 400–800 m dominates changes in salinity gradients between the two boundaries (r = 0.8, p < 0.005) and the MOC_S changes (r = 0.8, p < 0.01), consistent with results from an ocean reanalysis product (Zou et al., 2020). Note that by construction, MOC_S depends on both salinity and velocity distributions, but here we find a dominant role of salinity, which alone explains 90% of the MOC_S variability, with velocity changes contributing negligibly (Figure S5 in Supporting Information S1).

The mean-state inflowing waters at the WGC are much warmer especially in the upper layer (with maximum θ ∼ 4–5℃ at σ < 27.7 kg m^{-3}, Figure 3; see also Figure S3 in Supporting Information S1); the outflowing waters at the LC are relatively cold and concentrate in the intermediate density layer (θ ∼ 3–3.5℃ at σ ∼ 27.7 – 27.8 kg m^{-3}). The temperature gradient between the boundary currents corresponds to a warm-to-cold transformation in the basin, and thus a positive MOC_θ. In contrast to salinity, the temperature gradient between the inflowing and outflowing waters remains largely unchanged from 2016 to 2019, resulting in comparable transport structures in temperature coordinates (Figure 3d), and thus corresponding to similar MOC_θ.

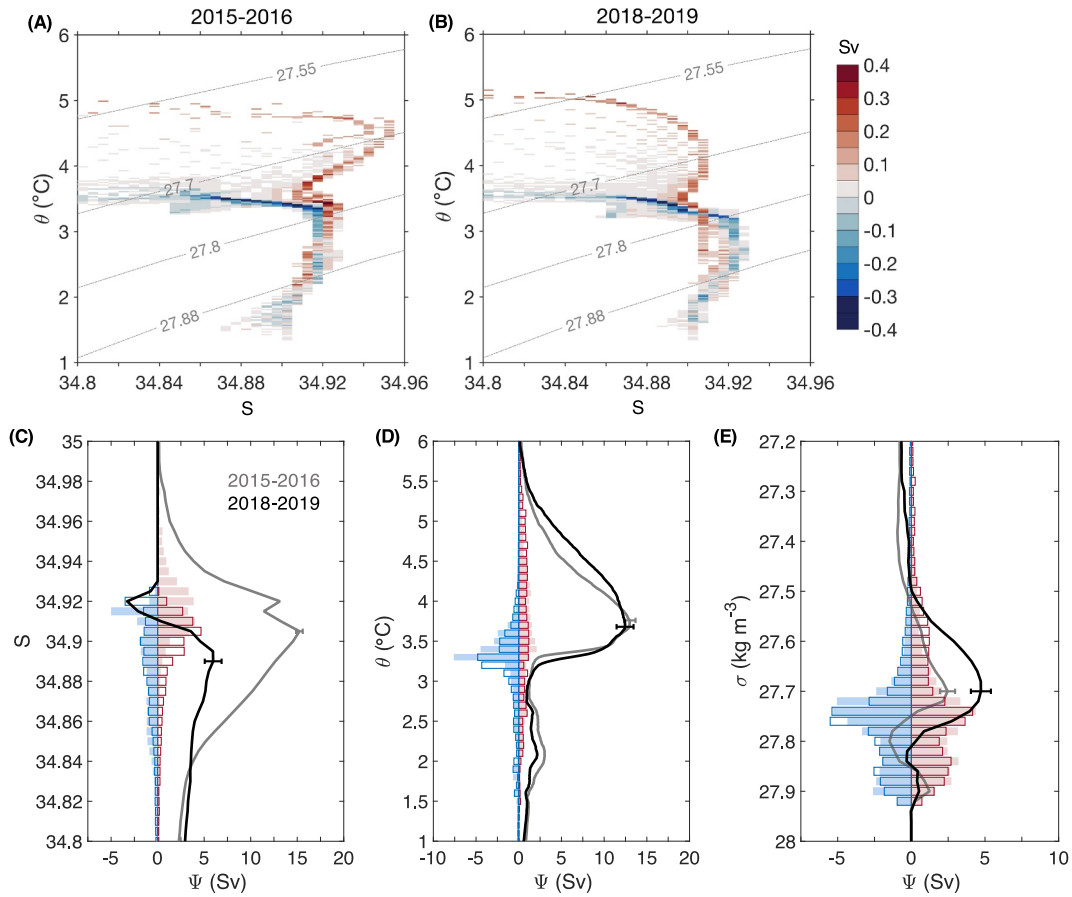

Figure 3. Mean volume transport across the OSNAP West section in individual potential temperature-salinity bins for (a) 2015–2016 and (b) 2018–2019, which correspond to the observed maximum and minimum MOC_S in Figure 2, respectively. Positive values indicate transport into the Labrador Sea. Gray dashed lines are contours of isopycnals (kg m^{-3}). (c) Mean volume transport profiles in salinity space (at intervals of 0.002). Transport of the inflowing/outflowing waters is indicated by red/blue bars (filled, 2015–2016; open, 2018–2019). The mean streamfunction (transport accumulated from high to low salinities) is indicated by solid lines, with the horizontal bar for uncertainty in the maximum transformation (plus/minus one standard error based on the monthly values). Panels (d, e) Similar to panel (c) but for transports in potential temperature, and potential density coordinates, respectively. For illustration purpose, the temperature interval is 0.1℃ in panel (d) and the density interval is 0.02 kg m^{-3} in panel (e).

The divergent salinity and temperature changes are then expected to generate density anomalies and impact MOC_σ. Particularly, a density decrease is observed at the subsurface WGC (−0.02 kg m^{-3} at 400–800 m) from 2016 to 2019, which arises mainly from a salinity decrease (−0.03) with negligible contribution from temperature change (Figure S6 in Supporting Information S1). The density decrease in the WGC then amplifies the density gradient between the two boundaries (i.e., the light WGC becomes even lighter) and thus strengthens the MOC_σ. Specifically, the density gradient in 2019 is nearly doubled of that in 2016, which, assuming a linear relationship between density gradients and the MOC_σ ($r = -0.8$, $p < 0.001$ during 2014–2020), would lead to a doubled MOC_σ (i.e., an increase of ~2 Sv), matching the observed change between the 2 years (Figure 3e). Altogether, the results indicate that WGC salinity anomaly is linked to the recent MOC_σ change in the Labrador Sea, through modifications of cross-basin salinity and density gradients.

3.3. Freshening and Overturning Response Over Recent Decades

We next extend the analysis to decadal-scale changes by assessing the impact of boundary salinity anomaly since the 1990s. Hydrographic data in the Labrador Sea reveal strong decadal salinity variability at the subsurface WGC, characterized by a salinification throughout the 2000s that peaks around 2010, followed by a freshening during the 2010s (Figure 4a). The boundary salinity variations follow the salinity distribution change during that

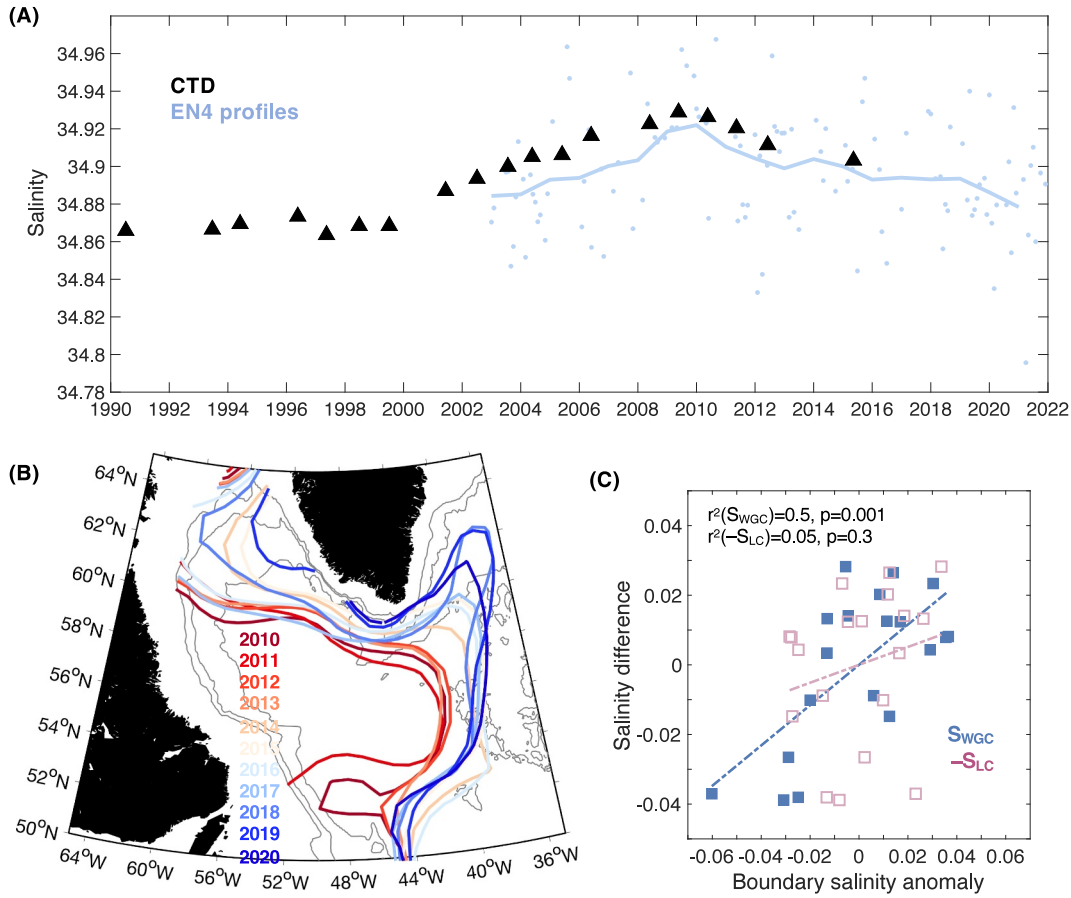

Figure 4. (a) Subsurface (400–800 m) salinity in the West Greenland Current (WGC) from various profile data. Black triangles indicate the CTD observations from AR7W repeat hydrography section. Blue dots indicate the monthly averages from nearby EN4 salinity profiles (see Figure 1a for location), and blue lines represent the annual averages. (b) Locations of the isohaline 34.89 averaged between 400 and 800 m for each year between 2010 and 2020 from EN4. (c) Relationship between the boundary salinity anomalies at the WGC/Labrador Current (LC) and the salinity differences between the boundaries, indicated by blue/purple squares. Dashed lines represent the fitted linear regression curve (with r^2 and *p*-value labeled). Data are from the CTD observations shown in panel (a).

period, as part of profound property variations having occurred throughout the subpolar basins (e.g., Chafik et al., 2019; Haine et al., 2023). In particular, the recent freshening at the subsurface WGC is associated with isohalines having gradually moved north-eastward, likely caused by large-scale gyre circulation changes (Figure 4b; e.g., Holliday et al., 2020).

Over those observed time scales, changes in salinity gradients between the boundaries exhibit a relatively stronger dependence on salinity anomaly at the WGC compared to the LC (Figure 4c), consistent with the picture of WGC-dominant salinity gradients identified during 2014–2020. These changes in salinity gradients reflect variations in the MOC_S and that in the overall strength of the basin's diahaline transformation as a steady state is expected to be reached over decadal time scales (Zou et al., 2024). A comparison of recent OSNAP observations with the inverse results from available CTD occupations (Figure 5) reveals a weaker MOC_S in the late 2010s (8.2 Sv) and a relatively stronger MOC_S in the late 2000s (14.6 Sv). The observed difference between the two periods is statistically significant at the 2 σ level (95%) given the error bars. Though it should be noted that the difference could be at least partially attributable to differences in the data sets and methods.

In the meantime, the change in the MOC_θ between the two periods is marginal (10.4 Sv in the late 2000s and 11.4 Sv in the late 2010s), indicating slight modification in temperature gradients across the basin. The contrasting haline and thermal changes produce density anomalies and thereby MOC_σ changes (Figure 5), which is relatively weak in the late 2000s (2.3 Sv) and becomes strengthened in the late 2010s (4.2 Sv). The increase in the

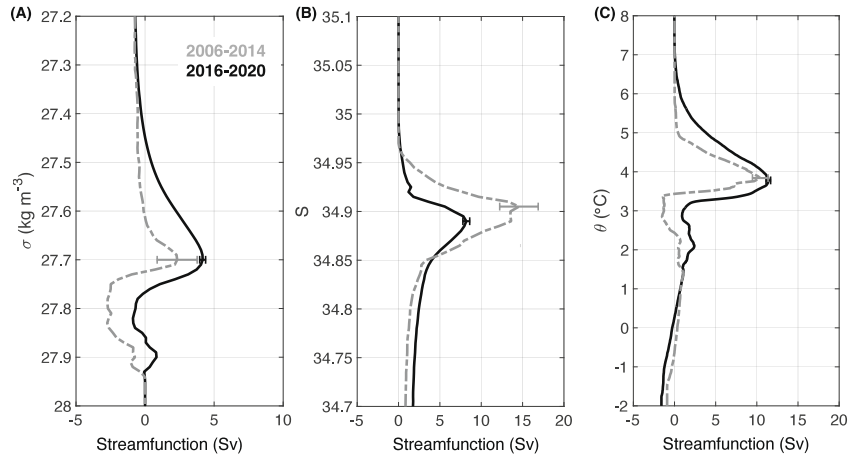

Figure 5. (a) Mean overturning streamfunction in potential density coordinates (integrated from the bottom upward) across the Labrador Basin during the late 2000s from the inverse method based on the CTD occupations (2006–2014, gray lines), and during the late 2010s from the OSNAP observations (2016–2020, black lines). Panels (b, c) are same as panel (a) but for salinity and potential temperature coordinates, respectively. Horizontal bars indicate the uncertainty of the maximum streamfunction (plus/minus one standard error based on the repeat CTD sections or the monthly values).

MOC_σ is of the same order of magnitude as its time-mean strength (~2 Sv) and is statistically distinct at the 1 σ level (67%) according to the error bars. The observations are also in line with previous reconstructions showing a weakening of the overturning from the 1990s to the 2000s followed by a strengthening to the 2010s at subpolar latitudes (e.g., Desbruyeres et al., 2019; Roussenov et al., 2022). Altogether, the results indicate that MOC_σ strengthens as MOC_S weakens. This reflects decadal changes in basin-scale transformation within the Labrador Sea, characterized by enhanced light-to-dense transformation alongside weakened salty-to-fresh transformation.

4. Conclusion and Discussions

We investigate the Labrador Sea overturning variability and its thermohaline attributions in recent decades, using a conjunction of historical hydrographic data and latest array measurements in the region. The results support a robust constraint on the time-mean overturning strength by the compensating salinity and temperature impacts on density from the 1990s to the 2010s, consistent with the unique feature of the Labrador Sea overturning as shown by previous observations over a limited time period (Zou et al., 2020, 2024). Furthermore, we present evidence for time-varying compensation that is responsible for the overturning strength varying over interannual and longer time scales, largely attributed to salinity anomalies at the basin's boundaries. Particularly, a fresher inflow via the WGC is linked to weaker salty-to-fresh water mass transformation in the Labrador Sea. This, combined with minimal changes in thermal transformation, leads to an enhanced light-to-dense water mass transformation and thus an increase in the overturning circulation in density space.

Our results are different from previous modeling studies that have emphasized an impact from surface salinity anomalies at subarctic-subpolar latitudes, in which a freshwater anomaly weakens the overturning by suppressing the open-ocean deep convection (e.g., Pontes & Menviel, 2024). Here, we highlight the role of subsurface salinity anomalies within the boundary current system, where a fresh anomaly is associated with enhanced overturning circulation in the Labrador Sea. At greater depths, a recent modeling work has shown that fresh anomalies may also strengthen overturning by reducing vertical stratification and thereby promoting deep convection (Wei & Zhang, 2024). Collectively, these studies underscore the subtle response of the Labrador Sea overturning circulation to salinity anomalies, which depends critically on their location and depth.

The apparent lack of coherence between the WGC and LC anomalies suggests distinct origins. Specifically, anomalies at the LC outflow can be attributed to anomalies advected from the WGC along the boundary current (Georgiou et al., 2021; Petit et al., 2023) or to those formed locally within the boundary current and through boundary-interior exchange (Georgiou et al., 2020; Palter et al., 2008; Zou et al., 2024). A further potential contribution from coastal meltwater has also been proposed (Bebieva & Lozier, 2023). Moreover, the highlighted role of the salinity anomaly at the WGC in determining the Labrador Sea changes involves a possible linkage to

upstream anomaly from the eastern subpolar basins, through the connection to the East Greenland Current (EGC). This is in line with modeling studies that have suggested a potential upstream source for Labrador Sea overturning variability (e.g., Menary et al., 2020; Roussenov et al., 2022). Altogether, a coherent picture of the overturning variability appears to establish across the Labrador and eastern subpolar basins, involving consistent anomalies propagating along the boundary current system of the subpolar gyre. As a follow-up study, we will incorporate more extensive regional observations to better diagnose the impact of coherent boundary changes on subpolar overturning variability.

The observed effect of salinity anomalies on the strength of the Labrador Sea overturning is manifested over the past two decades, likely owing to profound decade-long salinity variations (Figure 4). By comparison, the relative contributions from salinity and temperature are difficult to delineate during the 1990s. This is indicated by the similar overturning strength in the 1990 and 2010s (difference <1 Sv), despite their distinctive hydrographic conditions (i.e., the 1990s is characterized by much colder and fresher conditions, e.g., Yashayaev & Loder, 2016). Further analysis shows that the 1990s′ transformations occurred at colder isotherms ($\theta \sim 3.5$℃) and fresher isohalines (S $\sim$ 34.86), with strong compensating effects on density anomalies that thus yield a comparable MOC_σ (2.6 Sv at $\sigma = 27.7$ kg m^{-3}). Moreover, the overturning circulation in the 1990s probably involved a stronger impact from large-scale velocity changes than that from property changes (e.g., Chafik et al., 2023; Robson et al., 2016). Because of the time-varying degree of density compensation arising from the varying contributions from property and circulation changes, caution should be taken when developing temperature- or salinity-based proxies for the Labrador Sea overturning variability over decadal time scales. Long-term and continuous observations in the region are key for a careful evaluation of the relative impact from the salinity versus temperature changes on longer time scales.

Conflict of Interest

The authors declare no conflicts of interest relevant to this study.

Data Availability Statement

The 2014–2020 OSNAP data used in this study are available via Fu et al. (2023a, 2023b). Repeat hydrographic data at AR7W are available via CCHDO (2023). EN.4.2.2 data (Good et al., 2013) are avaiable at https://www.metoffice.gov.uk/hadobs/en4/ and are © British Crown Copyright, Met Office, 2013, provided under a Non-Commercial Government Licence http://www.nationalarchives.gov.uk/doc/non-commercial-government-licence/version/2/. World Ocean Atlas 2018 temperature (Locarnini et al., 2019) and salinity (Zweng et al., 2019) are accessible at https://www.ncei.noaa.gov/data/oceans/woa/WOA18/DATA/.

Acknowledgments
F. L. and S. Z. acknowledge support from the National Key Research and Development Program of China (Grant 2023YFF0805102). S. Z. also acknowledges support from National Natural Science Foundation of China (Grant 42376005). F. L. is also supported by the Fundamental Research Funds for the Central Universities (Grant 20720240100). Y. F. acknowledges funding from the U.S. National Science Foundation (OCE-1948335, OCE-2400434). T. P. is supported by Natural Environment Research Council grants RAPID Evolution (NE/Y003551/1) and ATLANTiS (NE/Y005589/1). OSNAP data were collected and made freely available by the Overturning in the Subpolar North Atlantic Program (OSNAP) project and all the national programs that contribute to it (www.o-snap.org).

References

Bebieva, Y., & Lozier, M. S. (2023). Fresh water and atmospheric cooling control on density-compensated overturning in the Labrador Sea. *Journal of Physical Oceanography*, *53*(11), 2575–2589. https://doi.org/10.1175/jpo-d-22-0238.1

Bretherton, F., Davis, R., & Fandry, C. (1976). A technique for objective analysis and design of oceanographic experiments applied to MODE-73. *Deep-Sea Research and Oceanographic Abstracts*, *23*(7), 559–582. https://doi.org/10.1016/0011-7471(76)90001-2

CCHDO Hydrographic Data Office. (2023). CCHDO hydrographic data archive. UC San Diego Library digital collections [Dataset]. https://doi.org/10.6075/J0CCHAM8

Chafik, L., Nilsen, J. E. Ø., Dangendorf, S., Reverdin, G., & Frederikse, T. (2019). North Atlantic Ocean circulation and decadal sea level change during the Altimetry Era. *Scientific Reports*, *9*(1), 1041. https://doi.org/10.1038/s41598-018-37603-6

Chafik, L., Penny Holliday, N., Bacon, S., Baker, J. A., Desbruyères, D., Frajka-Williams, E., & Jackson, L. C. (2023). Observed mechanisms activating the recent subpolar North Atlantic Warming since 2016. *Philosophical Transactions of the Royal Society A*, *381*(2262), 20220183. https://doi.org/10.1098/rsta.2022.0183

Curry, A. E., Hafatz, J., Kallan, M. J., Winston, F. K., & Durbin, D. R. (2011). Prevalence of teen driver errors leading to serious motor vehicle crashes. *Accident Analysis & Prevention*, *43*(4), 1285–1290. https://doi.org/10.1016/j.aap.2010.10.019

Desbruyères, D. G., Maze, G., Daniault, M., & Daniault, N. (2019). Surface predictor of overturning circulation and heat content change in the subpolar North Atlantic. *Ocean Science*, *15*(3), 809–817. https://doi.org/10.5194/os-15-809-2019

Fu, Y., Li, F., Karstensen, J., & Wang, C. (2020). A stable Atlantic meridional overturning circulation in a changing North Atlantic Ocean since the 1990s. *Science Advances*, *6*(48), eabc7836. https://doi.org/10.1126/sciadv.abc7836

Fu, Y., Lozier, M. S., Biló, T. C., Bower, A. S., Cunningham, S. A., Cyr, F., et al. (2023). Meridional Overturning Circulation observed by the Overturning in the Subpolar North Atlantic Program (OSNAP) array from August 2014 to June 2020 [Dataset]. https://doi.org/10.35090/gatech/70342

Fu, Y., Lozier, M. S., Biló, T. C., Bower, A. S., Cunningham, S. A., Cyr, F., et al. et al. (2023a). Seasonality of the meridional overturning circulation in the subpolar North Atlantic. *Communications Earth & Environment*, *4*(1), 181. https://doi.org/10.1038/s43247-023-00848-9

Georgiou, S., Ypma, S. L., Brüggemann, N., Sayol, J. M., Pietrzak, J. D., & Katsman, C. A. (2020). Pathways of the water masses exiting the Labrador Sea: The importance of boundary–interior exchanges. *Ocean Modelling*, *150*, 101623. https://doi.org/10.1016/j.ocemod.2020.101623

Georgiou, S., Ypma, S. L., Brüggemann, N., Sayol, J.-M., van der Boog, C. G., Spence, P., et al. (2021). Direct and indirect pathways of convected water masses and their impacts on the overturning dynamics of the Labrador Sea. *Journal of Geophysical Research: Oceans*, *126*(1), e2020JC016654. https://doi.org/10.1029/2020jc016654

Good, S. A., Martin, M. J., & Rayner, N. A. (2013). EN4: Quality-controlled ocean temperature and salinity profiles and monthly objective analyses with uncertainty estimates. *Journal of Geophysical Research: Oceans*, *118*(12), 6704–6716. https://doi.org/10.1002/2013jc009067

Haine, T. W. N., Siddiqui, A. H., & Jiang, W. (2023). Arctic freshwater impact on the Atlantic Meridional Overturning Circulation: Status and prospects. *Philosophical Transactions of the Royal Society A*, *381*(2262), 20220185. https://doi.org/10.1098/rsta.2022.0185

Holliday, N. P., Bersch, M., Berx, B., Chafik, L., Cunningham, S., Florindo-López, C., et al. (2020). Ocean circulation causes the largest freshening event for 120 years in eastern subpolar North Atlantic. *Nature Communications*, *11*(1), 585. https://doi.org/10.1038/s41467-020-14474-y

Jackson, L. C., Peterson, K. A., Roberts, C. D., & Wood, R. A. (2016). Recent slowing of Atlantic overturning circulation as a recovery from earlier strengthening. *Nature Geoscience*, *9*(7), 518–522. https://doi.org/10.1038/ngeo2715

Li, F., Lozier, M. S., Bacon, S., Bower, A. S., Cunningham, S. A., de Jong, M. F., et al. (2021). Subpolar North Atlantic western boundary density anomalies and the Meridional Overturning Circulation. *Nature Communications*, *12*(1), 3002. https://doi.org/10.1038/s41467-021-23350-2

Li, F., Lozier, M. S., & Johns, W. E. (2017). Calculating the meridional volume, heat, and freshwater transports from an observing system in the subpolar North Atlantic: Observing system simulation experiment. *Journal of Atmospheric and Oceanic Technology*, *34*(7), 1483–1500. https://doi.org/10.1175/jtech-d-16-0247.1

Locarnini, R. A., et al. (2019). *World Ocean Atlas 2018 volume 1: Temperature* (Vol. 1). NOAA Atlas NESDIS 81. https://doi.org/10.25923/e5rn-9711

Lozier, M. S., Li, F., Bacon, S., Bahr, F., Bower, A. S., Cunningham, S. A., et al. (2019). A sea change in our view of overturning in the subpolar North Atlantic. *Science*, *363*(6426), 516–521. https://doi.org/10.1126/science.aau6592

Mackay, N., Wilson, C., Holliday, N. P., & Zika, J. D. (2020). The observation-based application of a regional thermohaline inverse method to diagnose the formation and transformation of water masses north of the OSNAP array from 2013 to 2015. *Journal of Physical Oceanography*, *50*(6), 1533–1555. https://doi.org/10.1175/jpo-d-19-0188.1

Menary, M. B., Hermansom, L., & Dunstone, N. J. (2016). The impact of Labrador Sea temperature and salinity variability on density and the subpolar AMOC in a decadal prediction system. *Geophysical Research Letters*, *43*(23), 12217–12227. https://doi.org/10.1002/2016gl070906

Menary, M. B., Jackson, L. C., & Lozier, M. S. (2020). Reconciling the relationship between the AMOC and Labrador Sea in OSNAP observations and climate models. *Geophysical Research Letters*, *47*(18), e2020GL089793. https://doi.org/10.1029/2020gl089793

Palter, J. B., Lozier, M. S., & Lavender, K. L. (2008). How does Labrador Sea water enter the deep Western boundary Current? *Journal of Physical Oceanography*, *38*(5), 968–983. https://doi.org/10.1175/2007jpo3807.1

Petit, T., Lozier, M. S., Rühs, S., Handmann, P., & Biastoch, A. (2023). Propagation and transformation of upper North Atlantic Deep Water from the subpolar gyre to 26.5°N. *Journal of Geophysical Research: Oceans*, *128*(8), e2023JC019726. https://doi.org/10.1029/2023jc019726

Pickart, R. S., & Spall, M. A. (2007). Impact of Labrador Sea convection on the north Atlantic meridional overturning circulation. *Journal of Physical Oceanography*, *37*(9), 2207–2227. https://doi.org/10.1175/jpo3178.1

Pontes, G. M., & Menviel, L. (2024). Weakening of the Atlantic Meridional Overturning Circulation driven by subarctic freshening since the mid-twentieth century. *Nature Geoscience*, *17*(12), 1291–1298. https://doi.org/10.1038/s41561-024-01568-1

Robson, J., Ortega, P., & Sutton, R. (2016). A reversal of climatic trends in the North Atlantic since 2005. *Nature Geoscience*, *9*(7), 513–517. https://doi.org/10.1038/ngeo2727

Roussenov, V. M., Williams, R. G., Lozier, M. S., Holliday, N. P., & Smith, D. M. (2022). Historical reconstruction of subpolar North Atlantic overturning and its relationship to density. *Journal of Geophysical Research: Oceans*, *127*(6), e2021JC017732. https://doi.org/10.1029/2021jc017732

Speer, K., & Tziperman, E. (1992). Rates of water mass formation in the North Atlantic Ocean. *Journal of Physical Oceanography*, *22*(1), 93–104. https://doi.org/10.1175/1520-0485(1992)022<0093:rowmfi>2.0.co;2

Walin, G. (1982). On the relation between sea-surface heat-flow and thermal circulation in the ocean. *Tellus*, *34*(2), 187–195. https://doi.org/10.3402/tellusa.v34i2.10801

Wei, X., & Zhang, R. (2024). Weakening of the AMOC and strengthening of Labrador Sea deep convection in response to external freshwater forcing. *Nature Communications*, *15*(1), 10357. https://doi.org/10.1038/s41467-024-54756-3

Wunsch, C. (1996). *The Ocean circulation inverse problem*. Cambridge Univ. Press.

Xu, X., Rhines, P. B., & Chassignet, E. P. (2016). Temperature–salinity structure of the North Atlantic Circulation and associated heat and freshwater transports. *Journal of Climate*, *29*(21), 7723–7742. https://doi.org/10.1175/jcli-d-15-0798.1

Yashayaev, I. (2024). Intensification and shutdown of deep convection in the Labrador Sea were caused by changes in atmospheric and freshwater dynamics. *Communications Earth & Environment*, *5*(1), 156. https://doi.org/10.1038/s43247-024-01296-9

Yashayaev, I., & Loder, J. W. (2016). Recurrent replenishment of Labrador Sea Water and associated decadal-scale variability. *Journal of Geophysical Research: Oceans*, *121*(11), 8095–8114. https://doi.org/10.1002/2016jc012046

Yeager, S., Castruccio, F., Chang, P., Danabasoglu, G., Maroon, E., Small, J., et al. (2021). An outsized role for the Labrador Sea in the multidecadal variability of the Atlantic overturning circulation. *Science Advances*, *7*(41), eabh3592. https://doi.org/10.1126/sciadv.abh3592

Yeager, S., & Danabasoglu, G. (2014). The origins of late-twentieth-century variations in the large-scale North Atlantic Circulation. *Journal of Climate*, *27*(9), 3222–3247. https://doi.org/10.1175/jcli-d-13-00125.1

Zou, S., Lozier, M. S., Li, F., Abernathey, R., & Jackson, L. (2020). Density-compensated overturning in the Labrador Sea. *Nature Geoscience*, *13*(2), 121–126. https://doi.org/10.1038/s41561-019-0517-1

Zou, S., Petit, T., Li, F., & Lozier, M. S. (2024). Observation-based estimates of water mass transformation and formation in the Labrador Sea. *Journal of Physical Oceanography*, *54*(7), 1411–1429. https://doi.org/10.1175/jpo-d-23-0235.1

Zweng, M. M., et al. (2019). World Ocean Atlas 2018 volume 2: Salinity (Vol. *2 50*). (NOAA Atlas NESDIS 81, 2019). https://doi.org/10.25923/9pgv-1224